



Contents

Foreword

137–140

IJMS special issue John R. Eyler – Guest editors' foreword

Nicolas C. Polfer, James E. Bruce

Curriculum Vitae

141–141

Curriculum Vitae: John R. Eyler

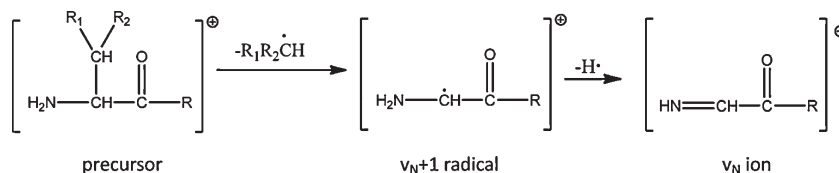
Regular Articles

142–154

Investigation of VUV photodissociation propensities using peptide libraries

Xiaohui Liu, Yong Fuga Li, Brian C. Bohrer, Randy J. Arnold,
Predrag Radivojac, Haixu Tang, James P. Reilly

► We study the VUV photodissociation of peptides found in synthetic libraries. ► The propensities for forming various unusual high-energy fragment ions are examined. ► The potential for using high-energy fragment ions in *de novo* sequencing is discussed.

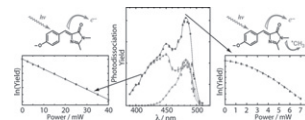


155–166

Photofragmentation of and electron photodetachment from a GFP model chromophore in a quadrupole ion trap

Matthew W. Forbes, Andrea M. Nagy, Rebecca A. Jockusch

► Photodissociation of the green fluorescent protein model chromophore in a QIT. ► Electron detachment requires a single visible photon. ► Photofragmentation requires multiple photons and is suppressed by collisions. ► Estimates are made for electron photodetachment and fragmentation cross sections.

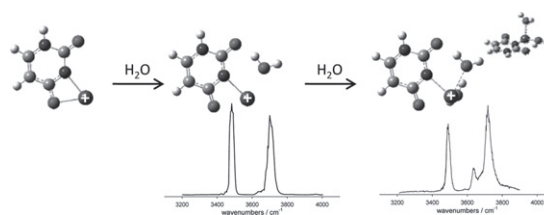


167–174

Structures of electrosprayed $\text{Pb}(\text{Uracil-H})^+$ complexes by infrared multiple photon dissociation spectroscopy

Osama Y. Ali, Travis D. Fridgen

► The IRMPD spectra of three complexes with a $[\text{Pb}(\text{Ura-H})]^+$ core have been recorded in the O-H/N-H stretch region. ► The computed spectra for the lowest energy structures agree very well with the experimental IRMPD spectrum. ► The $[\text{Pb}(\text{Ura-H})]^+$ core is deprotonated at N3 and has lead bound to either N3 and O4 or N3 and O2. ► The $[\text{Pb}(\text{Ura-H})]^+$ structure deprotonated at N1 with lead bound to N1 and O2 is not observed. ► $[\text{Pb}(\text{Ura-H})(\text{Ura})]^+$ was found to have four-coordinate lead. ► Water in hydrated complexes are directly coordinated to lead, the first also intramolecularly hydrogen bonded.

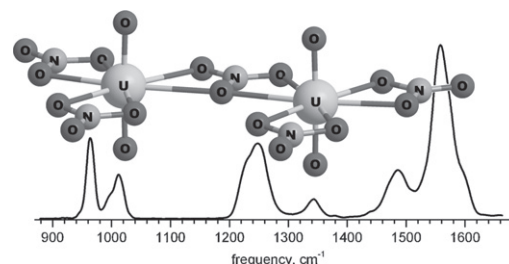


175–180

The gas-phase *bis*-uranyl nitrate complex $[(\text{UO}_2)_2(\text{NO}_3)_5]^-$: Infrared spectrum and structure

Gary S. Groenewold, Michael J. van Stipdonk, Jos Oomens, Wibe A. de Jong, Michael E. McIlwain

► The structure of the $[(\text{UO}_2)_2(\text{NO}_3)_5]^-$ cluster was deduced using IRMPD and DFT. ► Cluster structure involves two uranyl nitrate molecules bridged by one nitrate. ► Uranium is less strongly coordinated compared to the tris-uranyl nitrate anion. ► Pendant nitrate ligands are more strongly coordinated.

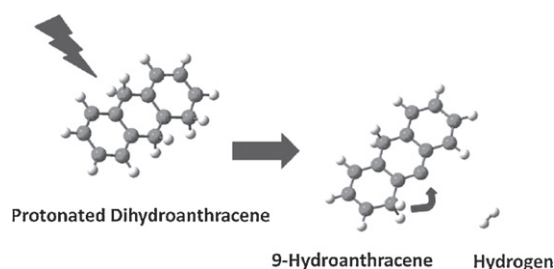


181–190

Formation of molecular hydrogen from protonated 9, 10-dihydroanthracene: Is the ejected H_2 rotationally and vibrationally excited?

Martin Vala, Jan Szczepanski, Jos Oomens

► Infrared multiphoton dissociation of protonated dihydroanthracene yields molecular hydrogen. ► After H_2 ejection, hydrogens shift about the carbon framework to produce 9-hydroanthracene. ► The H_2 is calculated to be asymmetrically ejected which may lead to its rovibrational excitation. ► Rotationally excited H_2 has been invoked to explain several important astronomical observations.

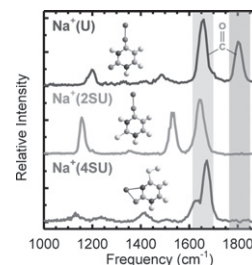


191–202

Infrared multiple photon dissociation action spectroscopy of sodiated uracil and thiouracils: Effects of thioketo-substitution on gas-phase conformation

Y.-w. Nei, T.E. Akinyemi, C.M. Kaczan, J.D. Steill, G. Berden, J. Oomens, M.T. Rodgers

- Sodium complexes of uracil and five thiouracils are examined by IRMPD spectroscopy.
- Binding of Na⁺ to the canonical tautomer is preferred for U, 2SU, 5Me2SU and 6Me2SU.
- Binding of Na⁺ to the minor 4-sulphydryl tautomer is preferred for 4SU and 24dSU.

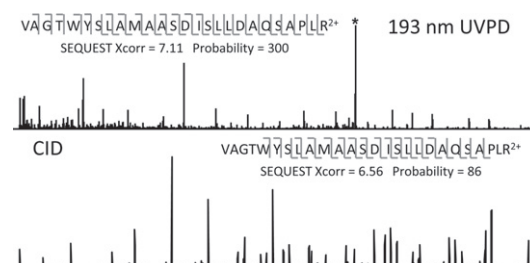


203–208

Analysis of protein digests by transmission-mode desorption electrospray ionization mass spectrometry with ultraviolet photodissociation

Jared B. Shaw, Jennifer S. Brodbelt

- Transmission mode DESI was utilized for a proteomics application.
- Confident protein identification is achieved through sequencing by tandem mass spectrometry.
- Ultraviolet photodissociation at 193 nm is compared to collision induced dissociation.

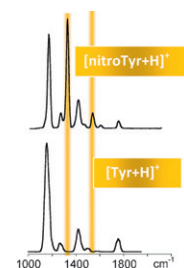


209–216

Tyrosine nitration as evidenced by IRMPD spectroscopy

Rajeev K. Sinha, Barbara Chiavarino, Maria Elisa Crestoni, Debora Scuderi, Simonetta Fornarini

- Protonated 3-nitrotyrosine is examined in 1000–2000 and 3200–3700 cm⁻¹ spectral ranges.
- Spectroscopic results are interpreted with the aid of quantum chemical calculations.
- IRMPD spectra of protonated 3-nitrotyrosine and protonated tyrosine ions are compared.
- Highly active modes diagnostic of the presence of the nitro group are revealed.

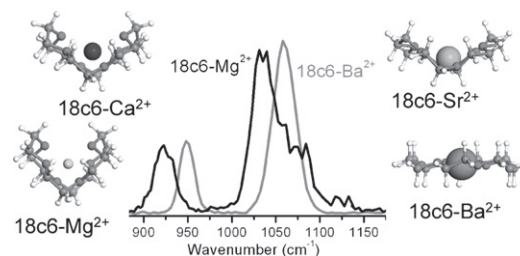


217–224

Vibrational study of isolated 18-crown-6 ether complexes with alkaline-earth metal cations

Francisco Gámez, Paola Hurtado, Bruno Martínez-Haya, Giel Berden, Jos Oomens

- We explore the structure of isolated 18-crown-6 ether (18c6) complexes with alkaline-earth divalent cations.
- Free-electron laser vibrational spectroscopy of the C–O and C–C stretching modes is performed.
- We find that symmetric molecular arrangements (point groups D₂, C₂, D_{3d}) dominate the conformational landscape.
- Large cations are bound in open conformations, small cations lead to cage-like inclusion complexes.

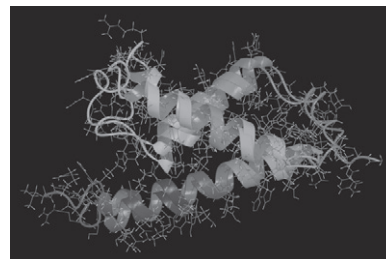


225–231

Investigating the gas phase structure of KIX with radical directed dissociation and molecular dynamics: Retention of the native structure

Xing Zhang, Ryan R. Julian

► Radical directed dissociation is used to examine protein structure in the gas phase. ► KIX is a three helix bundle protein that retains its native structure in the gas phase. ► Various electrostatic forces stabilize the native structure in the gas phase.

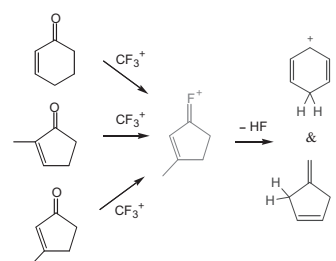


232–238

Fluoronium metathesis and rearrangements of fluorine-stabilized carbocations

Jos Oomens, Thomas Hellman Morton

► Halonium metathesis of CF_3^+ with 3-methylcyclopentenone gives the most stable $\text{C}_6\text{H}_8\text{F}^+$. ► CF_3^+ also gives the most stable isomer with cyclohexenone and 2-methylcyclopentenone. CF_3^+ reacts with conjugated enones to give C_6H_7^+ , which forms via HF loss from $\text{C}_6\text{H}_8\text{F}^+$. ► The C_6H_7^+ ion is a mixture of protonated benzene plus protonated fulvene. ► The most stable $\text{C}_6\text{H}_8\text{F}^+$ cannot lose HF to give either C_6H_7^+ isomer without rearranging.

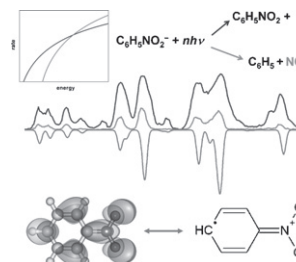


239–252

Spectroscopically resolved competition between dissociation and detachment from nitrobenzene radical anion

Jeffrey D. Steill, Jos Oomens

► Gas-phase IR action spectrum of nitrobenzene anion. ► Strong resonance interaction of nitro and phenyl groups. ► DFT calculations of energies and vibrations of nitrobenzene neutral and anion. ► Detailed spectral assignments and comparison to previous experiments. ► Statistical model of competition between dissociation and electron detachment.

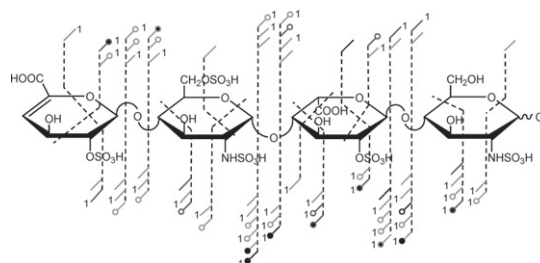


253–259

Electron detachment dissociation and infrared multiphoton dissociation of heparin tetrasaccharides

Franklin E. Leach III, Zhongping Xiao, Tatiana N. Laremore, Robert J. Linhardt, I. Jonathan Amster

► Ionized Sulfate Criteria defined; succinctly describes the ionic nature of a GAG. ► Heparin oligosaccharides, the most complex GAGs, are analyzed both by EDD and IRMPD. ► Cross-ring cleavages and glycosidic bond dissociation are produced by EDD and IRMPD.

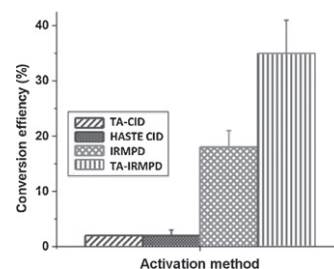


260–264

Tandem mass spectrometric methods for the analysis of iTRAQ labeled peptides in a quadrupole ion trap

Atim A. Entyenihi, John R. Griffiths, Gary L. Glish

- iTRAQ with a quadrupole ion trap. ► High iTRAQ reporter ion conversion efficiency with IRMPD.
- Methods to decrease the low-mass cut-off in MS/MS experiments using a quadrupole ion trap mass spectrometer.

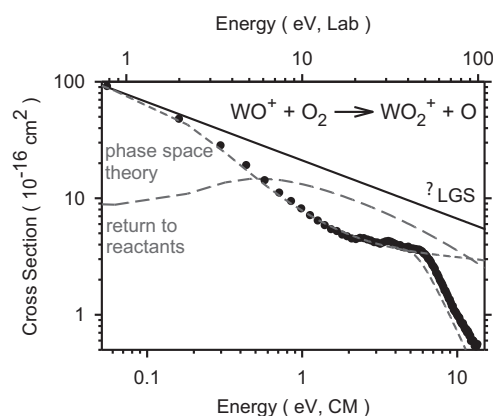


265–274

Collision-induced dissociation of MO^+ and MO_2^+ ($\text{M} = \text{Ta}$ and W): Metal oxide and dioxide cation bond energies

Christopher S. Hinton, Murat Citir, Manuel Manard, P.B. Armentrout

- In this study, we examine the collision-induced dissociation of tantalum and tungsten monoxides and dioxide cations. ► Reactions of tantalum and tungsten monoxide cations with molecular oxygen are studied. ► Bond energies for tantalum and tungsten monoxides and dioxide cations are determined and compared to theoretical and literature values. ► The dioxide cation thermochemistry determined here is much more precise than any previous determinations.

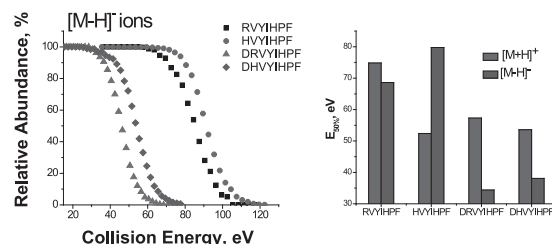


275–280

Energetics and dynamics of dissociation of deprotonated peptides: Fragmentation of angiotensin analogs

Julia Laskin, Zhibo Yangt

- We examined energy and entropy effects in dissociation of deprotonated peptides using surfaceinduced dissociation combined with RRKM modeling. ► Relative stability of peptides towards fragmentation is very different for protonated and deprotonated species. ► Fragmentation of acidic peptides is associated with very low threshold energy and tight transition state. ► Charge-remote fragmentation is observed for low-energy pathways of the basic RVIHPF peptide. ► Backbone fragmentation is characterized by fairly high energy barrier.

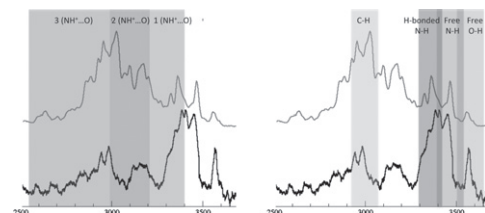


281–288

N-H⁺ vibrational anharmonicities directly revealed from DFT-based molecular dynamics simulations on the Ala_7H^+ protonated peptide

Amel Sediki, Lavina C. Snoek, Marie-Pierre Gaigeot

- First principle DFT-based dynamics of the protonated Ala_7H^+ peptide investigated at room temperature on a pico-second time-scale. ► The statistically most relevant conformations of Ala_7H^+ display two N-H⁺ ··· O-C hydrogen bonds on average. ► N-H⁺ stretching vibrational anharmonic movements revealed. ► The dynamical spectrum extracted from the DFT-based dynamics match extremely well the experimental IR-MPD spectrum. ► We have uncovered three separate signatures of N-H⁺ depending whether it is involved in one, two or three H-bonds with surrounding C=O groups.

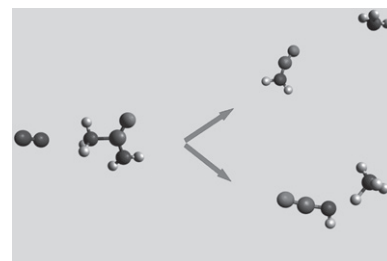


289–298

Collision induced dissociation of protonated urea with N_2 : Effects of rotational energy on reactivity and energy transfer via chemical dynamics simulations

Yannick Jeanvoine, Marie-Pierre Gaigeot, William L. Hase, Kihyung Song, Riccardo Spezia

- A QM/MM chemical dynamics of protonated urea with a diatomic projectile (N_2) is presented.
- An analytical N_2 /interaction potential for collision is developed, useful also for other related systems.
- Energy transfer and reactivity depends on the rotational energy of the projectile.
- A highest rotational activation of the ion favours the formation of high energy fragmentation products.

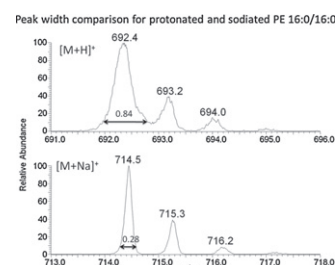


299–306

Characterization of protonated phospholipids as fragile ions in quadrupole ion trap mass spectrometry

Timothy J. Garrett, Matthew Merves, Richard A. Yost

- We examine the ion fragility of protonated and sodiated ions for phospholipids.
- We introduce experiments for ion fragility determination in ion transport.
- The sodiated ions are more stable under mass analysis and ion transport.

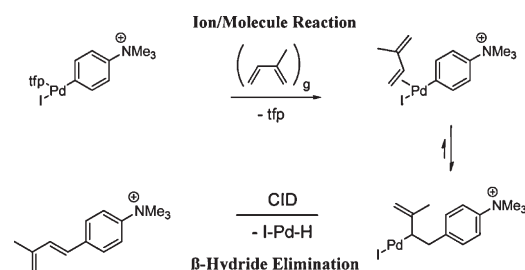


307–310

Heck coupling in the gas phase: Examination of the reaction mechanism by ion/molecule reactions and mass spectrometry

Lukas Fiebig, Hans-Günther Schmalz, Mathias Schäfer

- Labile Heck coupling reaction intermediates and the coupling product are investigated in the gas phase.
- Charge-tagging, ESI-MSⁿ, ion/molecule reactions and exact ion mass measurements are performed.
- A LTQ-Orbitrap Instrument is modified for the study.
- The results suggest that the Heck reaction proceeds via the accepted mechanism in solution and in the gas phase.

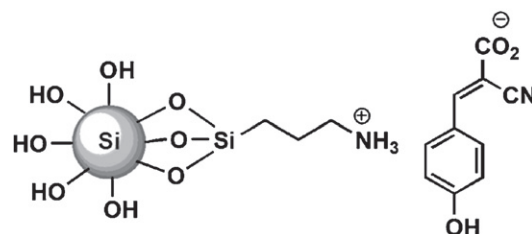


311–315

Modified silica-containing matrices towards the MALDI-TOF-MS detection of small molecules

Conor P. Mullens, Sreenivasa R. Anugu, Waldemar Gorski, Stephan B.H. Bach

- Immobilization of CHCA on silica with retention of 328 nm absorption.
- Reduction of low mass cationic interferences using the mesoporous silica.
- The SBA-15-CHCA matrix gives the best MALDI-TOF results for dopamine and serotonin.
- Method of preparing SBA-15-CHCA is simple and matrix has a long shelf life.

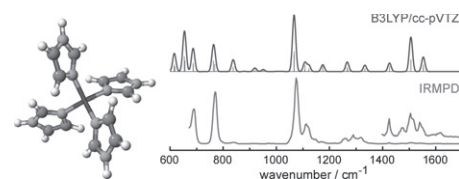


316–329

IR spectroscopy of isolated metal–organic complexes of biocatalytic interest: Evidence for coordination number four for $\text{Zn}^{2+}(\text{imidazole})_4$

Anita Lagutschenkova, Ulrich Joseph Lorenz, Otto Dopfer

► IR spectroscopic and mass spectrometric characterization of $[\text{ZnIm}_n]^{2+}$ complexes. ► First experimental characterization of Zn^{2+} –imidazole interaction in the gas phase. ► Evidence for tetrahedral coordination number $\text{CN} = 4$ in $[\text{ZnIm}_n]^{2+}$ complexes. ► Systematic trends of Zn^{2+} –Im interaction in $[\text{ZnIm}_n]^{2+}$ complexes with $n = 1$ –4. ► Biochemical implications for Zn enzymes.

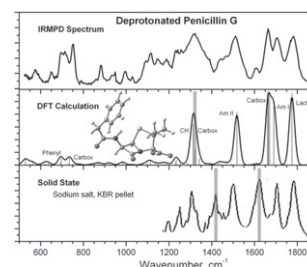


330–337

IRMPD spectroscopic investigation of gas-phase complexes of deprotonated penicillin G with Ba^{2+} , Zn^{2+} and Cd^{2+}

Robert C. Dunbar, Jos Oomens, Galina Orlova, Diethard K. Bohme

► IRMPD spectra of deprotonated penicillin G complexes with metal ions. ► Bare penicillinate anion spectrum agrees with calculation. ► Barium(II) complex has predicted structure chelating 3 oxygen sites. ► Zinc(II) complex spectrum suggests similar structure, but rearrangement is possible. ► Cadmium(II) complex rearranges depending on electrospray solvent.

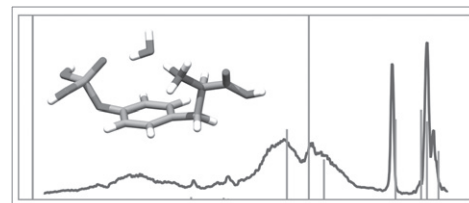


338–347

Structure of singly hydrated, protonated phospho-tyrosine

D. Scuderi, J.M. Bakker, S. Durand, P. Maitre, A. Sharma, J.K. Martens, E. Nicol, C. Clavaguéra, G. Ohanessian

► We use IRMPD spectroscopy in both the fingerprint and X–H stretching regions. ► We compare the spectra of singly hydrated and bare phosphorylated tyrosine. ► MP2 quantum calculations are used to assign structures based on IR spectra. ► Water bridges between the amino acid and phosphate functions.

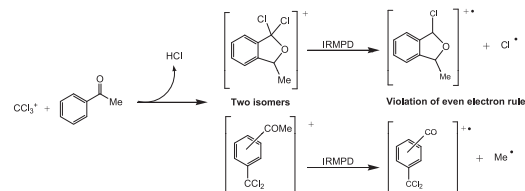


348–356

The ion/molecule reactions of CCl_3^+ with acetophenones

Tatiana Giroldo, Camila Bacellar Cases da Silveira, José M. Riveros

► CCl_3^+ reacts with acetophenone in the gas-phase through three different channels. ► One of the main reaction products, $\text{C}_9\text{H}_7\text{Cl}_2\text{O}^+$, presents an interesting structural problem. ► IRMPD of $\text{C}_9\text{H}_7\text{Cl}_2\text{O}^+$ ions proceeds by loss of either Cl or CH_3 in violation of the even-electron rule. ► Theoretical calculations and reactivity studies clearly show the formation of two isomeric $\text{C}_9\text{H}_7\text{Cl}_2\text{O}^+$ ions.



357–361**Identification of phosphorylated human peptides by accurate mass measurement alone**

Yuan Mao, Leonid Zamdborg, Neil L. Kelleher,
Christopher L. Hendrickson, Alan G. Marshall

- Peptide phosphorylation can be detected by mass alone. ► For mass error ± 50 ppb, 95% of all phosphorylated human tryptic peptides can be distinguished from nonmodified peptides.
- Phosphopeptide precursor ions in MS1 can be selected for selected dissociation in MS2.

